THE JOURNAL OF PHYSICAL CHEMISTRY B

Article

pubs.acs.org/JPCB

Reactive Dynamics Study of Hypergolic Bipropellants: Monomethylhydrazine and Dinitrogen Tetroxide

Yi Liu,*[,†,‡] Sergey V. Zybin,[‡] Jiaqi Guo,[‡] Adri C. T. van Duin,[§] and William A. Goddard, III*[,‡]

[†]School of Materials Science and Engineering, University of Shanghai for Science and Technology, 516 Jungong Road, Shanghai 200093, P. R. China

[‡]Materials and Process Simulation Center, 139-74, California Institute of Technology, Pasadena, California 91125, United States

[§]Department of Mechanical and Nuclear Engineering, Pennsylvania State University, University Park, Pennsylvania 16802, United States

ABSTRACT: To gain an atomistic-level understanding on physical and chemical processes occurring at the interfaces of hypergolic propellants, we carried out the first reactive dynamic (ReaxFF) simulations to study the reactive hypergolic mixture of monomethylhydrazine (MMH) and dinitrogen tetroxide (NTO), in comparison with the ethanol (EtOH) and NTO mixture that is reactive but nonhypergolic. Our studies show that the MMH−NTO mixture releases energy more rapidly than the EtOH−NTO mixture upon mixing the fuels and oxidizers. We found that the major early chemical reactions between MMH and NTO are hydrogen abstractions and N−N bond scissions. The MMH−NTO mixture has more reaction channels than EtOH−NTO based on statistical analyses of chemical reaction events and channels at early stages of the dynamics. Analyzing the evolution of product distribution over reaction time shows that the oxidizer (NO_2) diffuses into the fuels (MMH or EtOH) for the occurrence of reactions, demonstrating the influence of physical mixing on chemical reactions. Our simulations suggest that effective hypergolic systems require fuels with low energy barriers of H abstractions and/or bond scissions and oxidizers with large diffusion mobility for efficient physical mixing.

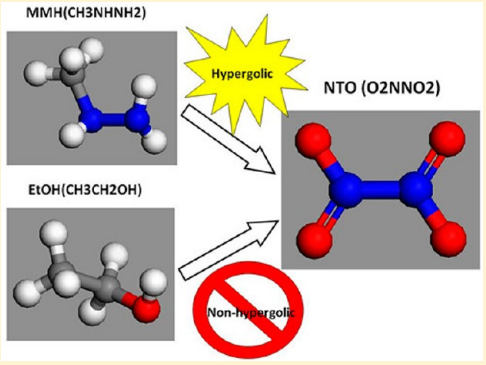

1. INTRODUCTION

Hypergolic propellants play vital roles in orbital maneuvering and reaction control systems in aerospace industries, including satellites, interplanetary vehicles, and reusable spacecrafts.[1] Hypergolic bipropellants consist of fuels and oxidizers that can ignite rapidly upon mixing within tens of milliseconds without the help of external ignition devices. This self-ignition feature of propellants improves the reliability of ignition in rocket engines. High density specific impulse and short ignition delay time are the primary performance requirements for hypergolic propellants. Hypergolic bipropellants normally consist of hydrazine or its derivative systems as fuel, while common oxidizers include hydrogen peroxide, dinitrogen tetroxide, and nitric acids.[2,3] While these fuels and oxidizers satisfy some flight performance requirements, they present ground safety hazards because of their toxic, corrosive, and carcinogenic properties. Safety precaution drives the search for the replacement of such toxic propellants with environmentally friendly ones such as ionic liquids.[4−12]

Monomethylhydrazine (MMH) and dinitrogen tetroxide (NTO) is one of the most utilized bipropellant combinations,[13−15] with high performance but suffering from the above-mentioned environmental problems. Toward designing "green" hypergolic propellants, Catoire and his colleagues[6] studied the possibility of replacing the toxic MMH fuel with ethanol (EtOH), while keeping the oxidizer NTO unchanged. Their experiments show that EtOH−NTO mixtures are not hypergolic but reactive at room temperature. Thus, the MMH−NTO and EtOH−NTO mixtures serve as good model systems for comparative study of hypergolicity because the two mixtures differ only in fuels. Moreover, MMH and EtOH molecules are similar in that they both have methyl groups.

Understanding the mechanism of self-ignition of hypergolic propellants, especially the early stage chemical reactions, helps develop a chemical kinetic model, which in turn can be used to predict the performance of fuel/oxidizer combinations and optimize the design of propulsion systems. The conventional theoretical approach to studying chemical dynamics is to perform quantum mechanical (QM) calculations on a large number of elemental model reactions, passing parameters into chemistry kinetics studies based on preassumed mechanistic models. This approach usually requires extensive and expensive QM calculations,[5,16] and its accuracy and reliability depends largely on the completeness of hypothesized mechanisms. Possible reaction mechanisms are usually too many to be explored completely due to a large number of reactions involved even for simple molecular systems. QM-based geometry optimizations or molecular dynamics methods can

Received: August 22, 2012
Revised: November 8, 2012
Published: November 13, 2012

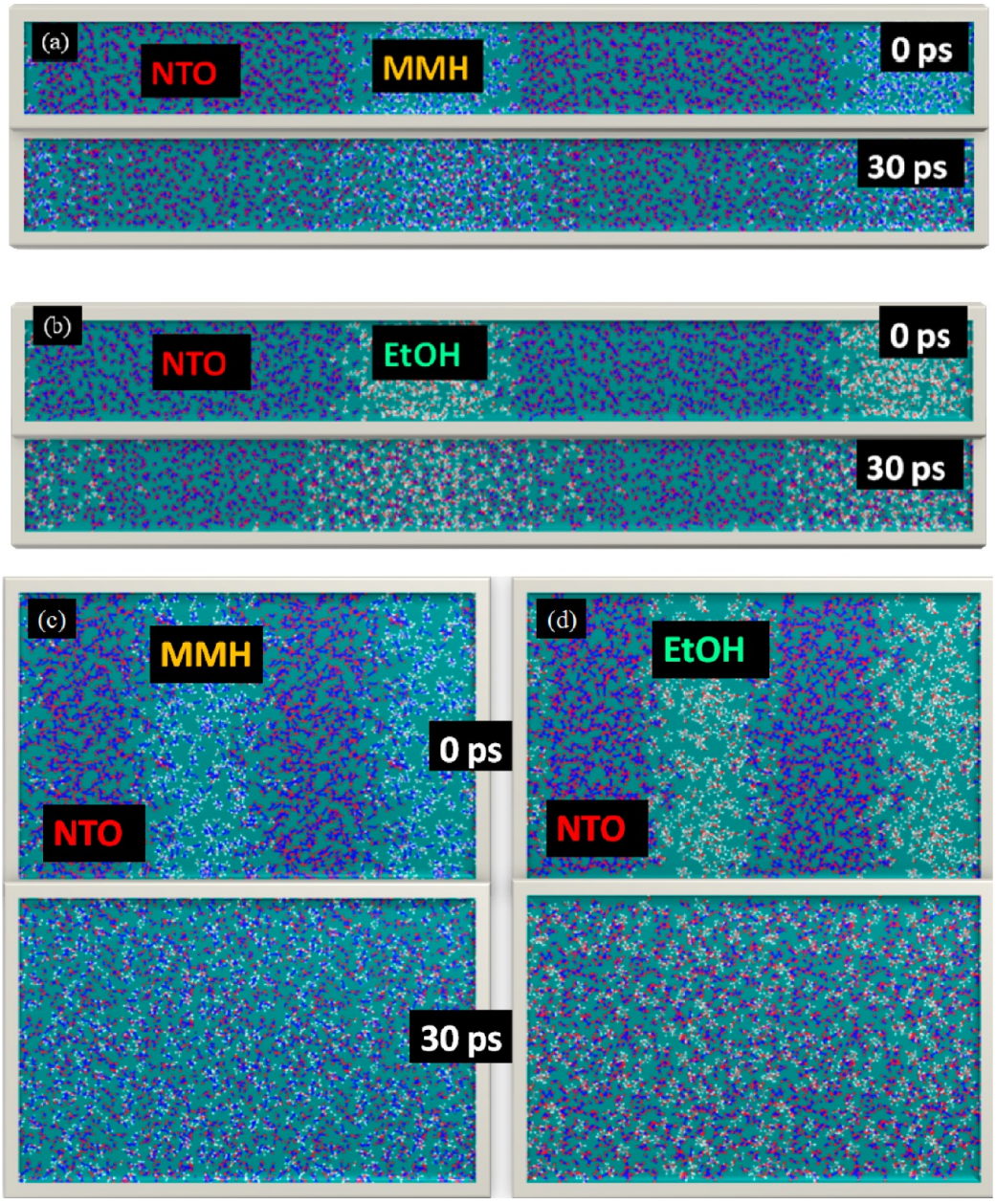

Figure 1. Periodic interface models of (a) MMH−NTO and (b) EtOH−NTO mixtures with small interfacial areas, and (c) MMH−NTO and (d) EtOH−NTO with large interfacial areas. The MD snapshots after 30 ps are also shown to illustrate the extent of liquid mixing.

only afford to study small molecules or model clusters in gas phase.[17−21]

Alternatively, reactive molecular dynamics using ReaxFF force field[22] is a direct dynamic approach to study large-scale chemical reactions at the atomistic level with a higher efficiency than quantum mechanics. ReaxFF dynamics can be used to study complex multimolecular reactions occurring in condensed phases at nanometer length scale and picosecond time scale with reasonable computing resources, taking into account temperature and pressure effects. ReaxFF had been previously applied to study energetic materials including RDX, PETN, and HMX,[23−34] demonstrating its capability of studying highly reactive organic systems.

In this work, we carried out, for the first time, a reactive molecular dynamics study of the hypergolic MMH−NTO bipropellant mixture, compared with the nonhypergolic but reactive EtOH−NTO mixture. We examined the physical processes and chemistry at the interface between fuels and oxidizers at an atomistic level, focusing on the differences between hypergolic and nonhypergolic systems. The rest of article is organized as follows: the computation models and simulation procedures are described in section II, followed by the results and discussions in section III. We draw conclusions in section IV.

2. MODELING AND COMPUTATIONAL PROCEDURES

We constructed the periodic atomic models including MMH (CH_3NH-NH_2, 128 molecules), EtOH (C_2H_5OH, 128 molecules), NTO (N_2O_4, 256 molecules), the mixture of MMH (128 molecules)−NTO (256 molecules), and the mixture of EtOH (128 molecules)−NTO (256 molecules). The NTO/MMH ratio adopted in our models is 2:1 since the

dx.doi.org/10.1021/jp308351g | J. Phys. Chem. B 2012, 116, 14136−14145

ratio in experimental MMH−NTO mixtures is 1.65 or 2.40.[1] The molecules were first randomly inserted into the simulation box. The systems then undergo five expansion-and-compression annealing cycles until the experimental densities are achieved: NTO at 1443 kg/m^3, EtOH at 789 kg/m^3, and MMH at 880 kg/m^3 at ambient conditions. We also studied these systems at half their experimental densities. To investigate the effects of mixing efficiency, we constructed two types of interface models, with large interfacial areas (MMH−NTO, 36 × 36 × 29 Å^3; EtOH−NTO, 36 × 36 × 30 Å^3 at the experimental densities) and small interfacial areas (MMH−NTO, 15 × 15 × 170 Å^3; EtOH−NTO, 15 × 15 × 176 Å^3 at their experimental densities), respectively, as shown in Figure 1. Comparative studies were also done between the cases with and without premixing of mixtures.

The simulation procedures in this work are as follows. We first equilibrated the systems by running energy minimization for 1 ps followed by NVT dynamics at 50 K for 0.5 ps. Then, the systems were heated from 50 to 3000 K at a rate of 1 K/fs. The temperature was controlled using the Berendsen method with a coupling constant of 0.1 ps. Finally, we ran molecular dynamics in the NVE or NVT ensembles for 120 ps at temperatures ranging from 1000 to 3000 K with 250 K increments. The high temperatures used in these simulations allowed the reactions to be completed in hundreds of picoseconds using affordable computing resources rather than milliseconds in laboratory experiments. The time step 0.1 fs was used for the integration of the equation of motion. The parallel ReaxFF simulations in this study were done with the GRASP program that was originally developed at the Sandia National laboratory by Aidan Thompson, then modified by the authors at Caltech. The thermodynamic properties, trajectory, and bond order were obtained directly from the reactive dynamics and were used in the analyses of energy release, temperature profile, chemistry, and product distributions.

3. RESULTS AND DISCUSSION

3.1. Energy Release and Temperature Evolution in NVE Dynamics. The time evolution of potential energy (E_p) directly reflects energy changes along with reaction dynamics. Figure 2a shows that E_p of pure NTO and EtOH systems level off during the NVE simulations, indicating that the fuel and the oxidizers alone do not react significantly under the studied conditions. In contrast, E_p of both fuel-oxidizer mixtures decreases significantly. Furthermore, E_p of the MMH−NTO mixture drops more rapidly than that of the EtOH−NTO mixture until around 50 ps, releasing 2.5 kcal/mol more energy per atom. E_p of the MMH−NTO mixture then rises slowly until 120 ps. However, the energy of EtOH−NTO drops quickly between 50 and 80 ps, followed by a slight rise until 120 ps.

The time evolution of temperatures, shown in Figure 2b, exhibits opposite behaviors compared to the evolution of potential energies due to total energy conservation in NVE dynamics. The temperatures of pure NTO and EtOH change very little essentially. In contrast, the temperature of the MMH−NTO mixture increases from 2000 to 4400 K, while the temperature of the EtOH−NTO mixture rises from 2000 to 3300 K after the first 50 ps. This indicates that the initial higher potential energy release in the MMH−NTO mixture leads to the higher temperature rise compared to the EtOH−NTO mixture. After 50 ps, the temperature of the EtOH−NTO

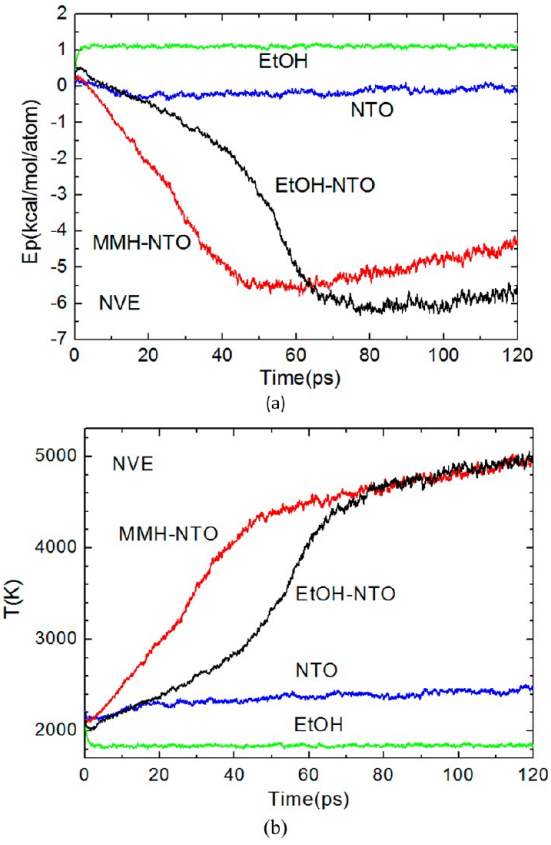

Figure 2. (a) Normalized potential energy and (b) temperature as a function of time in the NVE dynamics with an initial temperature T = 2200 K. The initial potential energy is set to zero as a reference.

mixture increases more rapidly and reaches 4600 K at 80 ps, close to the maximum temperature of the MMH−NTO.

3.2. Reaction Products in NVE Dynamics. Analyzing chemical species produced during the course of dynamics helps to understand the evolution of chemical processes. Figure 3 shows the time evolution of chemical products in the NVE dynamics. For the MMH−NTO mixture, the NO_2 product increases first and dramatically due to NTO decomposition, and then decreases gradually until 50 ps due to redox reactions. We found that N_2, H_2O, CO_2, and O_2 molecules increase to their maximum counts after the first 50 ps. Since these chemical species are stable reaction products, the product profiles indicate that most endothermic reactions were completed within 50 ps. Indeed, the evolution of reaction products is consistent with the potential energy release and temperature rise shown in Figure 2.

From 50 to 120 ps, we found that the amount of H_2O decreases and OH increases slightly. This indicates that some water molecules were further decomposed at 4400 K, leading to the rise of potential energy. The water dissociation was also found in the first-principles molecular dynamics study of PETN[35] where temperature reaches between 3000 and 4200 K. Consequently, the unstable OH radicals could be involved in subsequent reactions to play roles of catalysts to drive high temperature dynamics further.

For the EtOH−NTO mixture, NO_2 increases quickly and maximizes at the first 5 ps. Then, NO_2 decreased gradually to <10% of the maximum amount until 80 ps. During this period, the potential energy dropped continuously. H_2O appears from the beginning and increases to its maximum quantity at 60 ps.

dx.doi.org/10.1021/jp308351g | J. Phys. Chem. B 2012, 116, 14136−14145

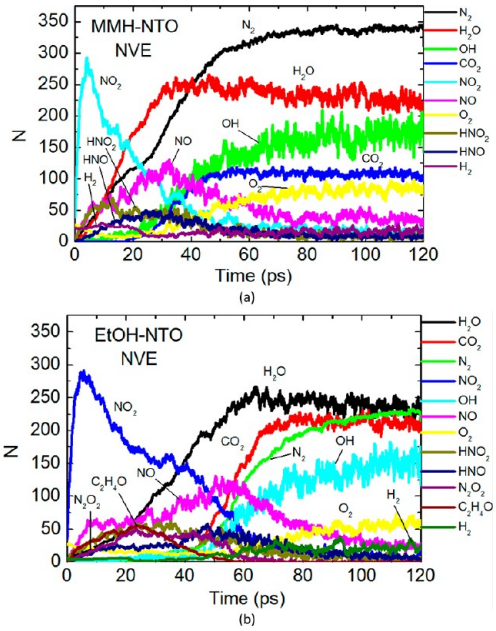

Figure 3. Number of chemical species as a function of time in the NVE dynamics for (a) MMH−NTO and (b) EtOH−NTO mixtures with an initial temperature T = 2000 K.

CO_2 and N_2 start to increase from 40 ps and level off around 80 ps. The chemical reactions that lead to the CO_2 and N_2 products cause the rapid potential energy drop between 40 and 80 ps.

3.3. Potential Energy and Reaction Products in NVT Dynamics. Figure 4 shows the time evolution of potential energy in NVT dynamics at T = 1000, 1500, and 2000 K. At T = 2000 K, E_p decreases more rapidly in the MMH−NTO than the EtOH−NTO mixture at the first 30 ps. Then, the E_p of both mixture systems drops at similar but slower rates. Figure 5 shows the evolution of chemical species in the NVT dynamics at T = 2000 K. It shows that the amount of NO_2 does not drop and N_2 does not increase significantly after 30 ps in the MMH−NTO mixture. Further analysis on the N_2 formation mechanisms reveals that successive H abstractions of MMH (CH_6N_2), mainly by NO_2 and OH, led to intermediate CH_3N_2 that decomposed further into N_2 and CH_3. However, little N_2 formed in the EtOH−NTO mixture, originating from NTO.

3.4. Mass Spectra. Mass spectra were computed for the chemical species found in reactive dynamics that allow direct comparisons with laboratory experimental findings. Figure 6 shows the predicted mass spectra from the NVE dynamics with initial T = 2200 K at half densities. For the MMH−NTO mixture, we found that the reactant peaks are NO_2 (m/e = 46), N_2O_4 (m/e = 92), and CH_6N_2 (m/e = 46). The peaks of products correspond to CH_3OH (m/e = 32), N_2 (m/e = 28), N_2O (m/e = 44), CO_2 (m/e = 44), and H_2O (m/e = 18), respectively. These chemical species were also found experimentally in the mass spectrum of reaction products of MMH and NTO. In addition, ReaxFF dynamics also predicted peaks corresponding to NO (m/e = 30), NO_3 (m/e = 62), HNO_2 (m/e = 47), CH_3 (m/e = 15), H_2 (m/e = 2), CH_4N_2 (m/e = 44), CH_4 (m/e = 16), and HNO_3 (m/e = 63) species. Many of these are intermediate species with short lifetimes that are difficult to detect in laboratory experiments.

For the EtOH−NTO mixture, major chemical species found in the ReaxFF dynamics include NO_2 (m/e = 46), C_2H_6O (m/e = 46), N_2O_4 (m/e = 92), NO_3 (m/e = 62), NO (m/e = 30), HNO_2 (m/e = 47), C_2H_4O (m/e = 44), H_2O (m/e = 18), HNO_3 (m/e = 63), C_2H_5O (m/e = 45), and C_2H_4 (m/e = 28).

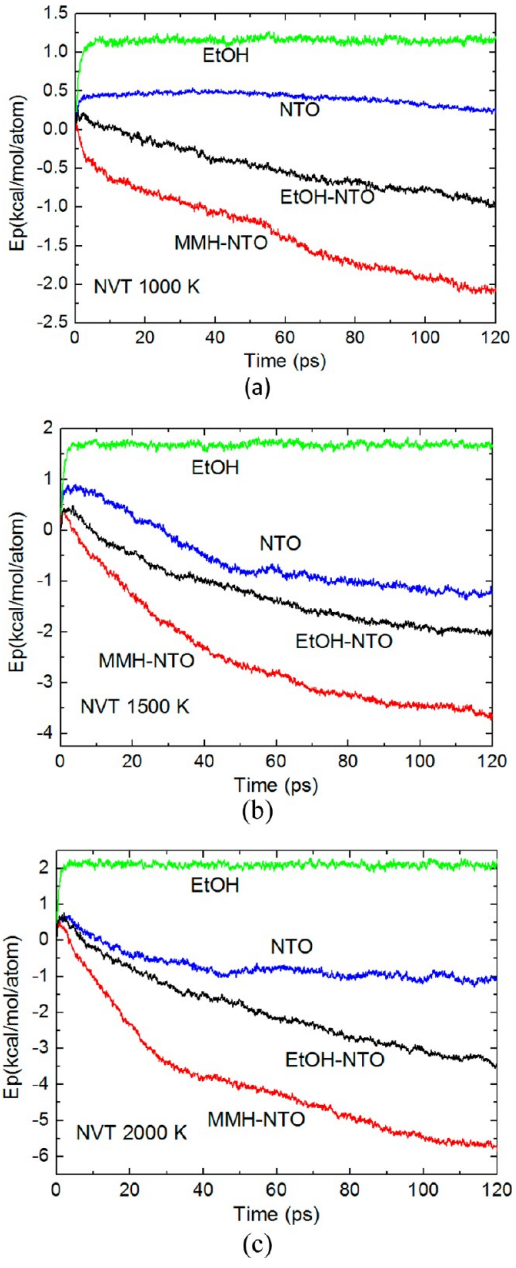

Figure 4. Normalized potential energy per atom as a function of time in the NVT dynamics at (a) 1000, (b) 1500, and (c) 2000 K. The initial potential energy is set to zero as a reference.

3.5. Chemical Reaction Rates. The decomposition of fuel molecules is the main cause of the early endothermic reactions during an induction period. The decomposition of fuel molecules happens exponentially. The rate of decay can be quantified by a characteristic time τ that depends on temperatures.[24] In Figure 7, we plot logarithmic characteristic time τ as a function of inverse temperature between 2000 and 3000 K. According to the Arrhenius theory, the energy barrier of initial decomposition can be estimated from the slope of the fitted straight line. Using the theory, we predict that the energy barrier of MMH decomposition is 22.9 kcal/mol, 3.8 kcal/mol lower than the EtOH decomposition barrier of 26.7 kcal/mol.

dx.doi.org/10.1021/jp308351g | J. Phys. Chem. B 2012, 116, 14136−14145

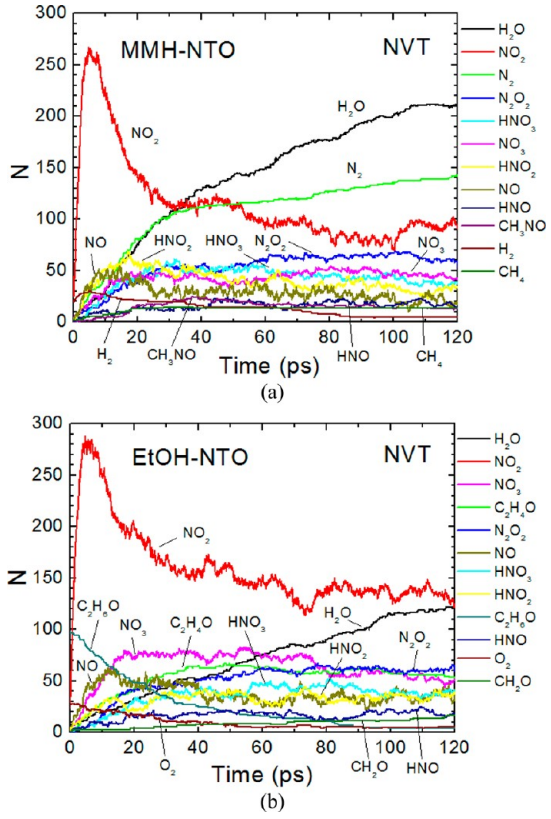

Figure 5. Number of chemical species as a function of time in the NVT dynamics at 2000 K for (a) MMH−NTO and (b) EtOH−NTO mixtures.

MMH decomposition rates are about three times faster than EtOH. Theses results indicate that the MMH fuel molecules in hypergolic mixtures decompose more easily than the EtOH fuel molecules in nonhypergolic mixtures.

After the induction period, potential energy drops exponentially, and overall, chemical reactions become exothermic. We calculated the characteristic reaction time τ that describes how fast the energy decays with time. Figure 8 shows the logarithmic characteristic reaction time as a function of inverse temperatures between 2000 and 3000 K. The linear relationship between characteristic time and inverse temperature indicates Arrhenius behavior where the slope of the fitted straight line gives the energy barrier of overall reactions. The calculated energy barrier is 15.5 kcal/mol for MMH−NTO mixtures. This is about 3.3 kcal/mol lower than the calculated energy barrier for EtOH−NTO mixtures, 18.8 kcal/mol, again indicating that MMH−NTO is more reactive than EtOH−NTO mixtures. The higher reactivity of the MMH−NTO mixture should contribute to its hypergolic nature. However, the nonhypergolic EtOH−NTO mixture exhibits relatively lower reactivity.

To examine the role of mixing efficiency, we built well-mixed mixture models before running reactive dynamics. As shown in Figure 8b, we calculated a reaction barrier of 15.1 kcal/mol for the premixed MMH−NTO mixture, similar to the interfacial models without premixing. For the EtOH−NTO mixture, the reaction barrier is 18.8 kcal/mol regardless of premixing. The reaction rate for EtOH−NTO is 80% slower than that of MMH−NTO. Our studies show that the models with and without premixing have similar energy barriers, indicating that premixing has negligible effects on the reactivity of mixtures. Since the nonpremixing large interface models have relatively

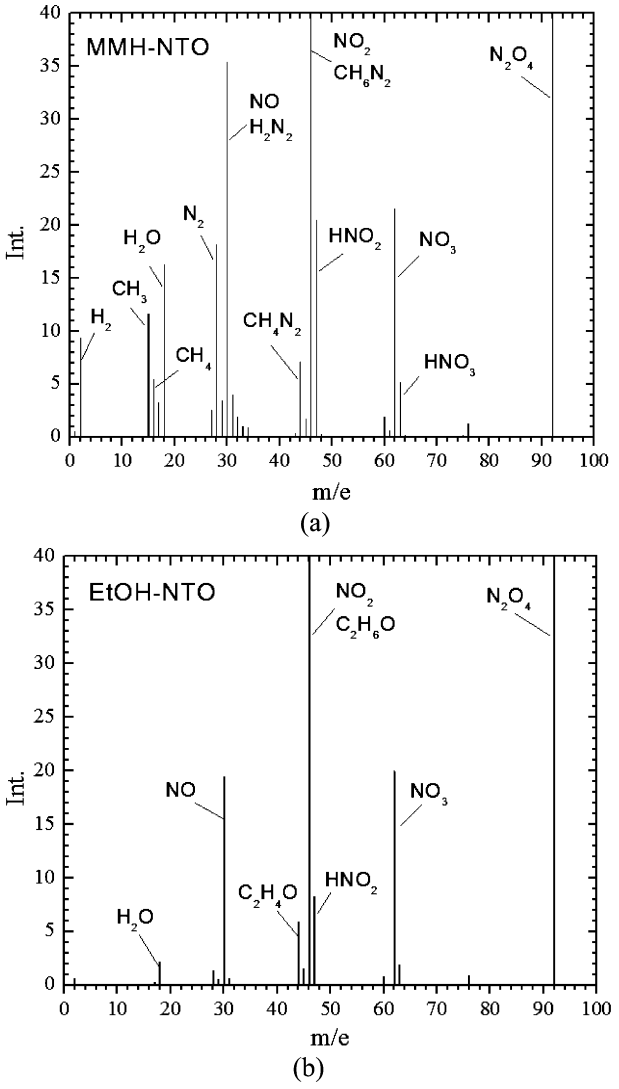

Figure 6. Predicted mass spectra from the ReaxFF NVE dynamics for (a) MMH−NTO and (b) EtOH−NTO mixtures at an initial T = 2200 K at half experimental densities.

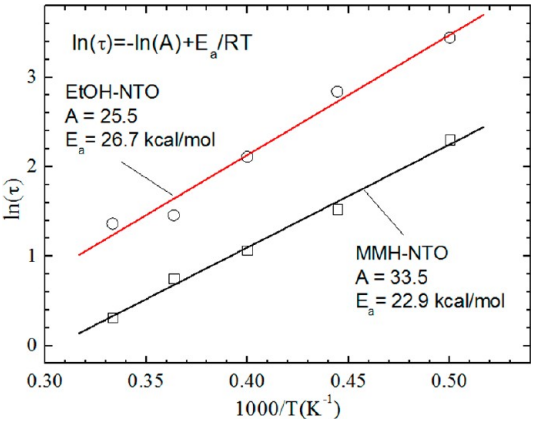

Figure 7. Logarithm characteristic reaction time as a function of inverse temperature (2000−3000 K) for the MMH−NTO and EtOH−NTO mixtures. The calculated energy barriers are 22.9 kcal/mol for MMH decomposition and 26.7 kcal/mol for EtOH decomposition. Insets are Arrhenius equations and fitted parameters.

dx.doi.org/10.1021/jp308351g | J. Phys. Chem. B 2012, 116, 14136−14145

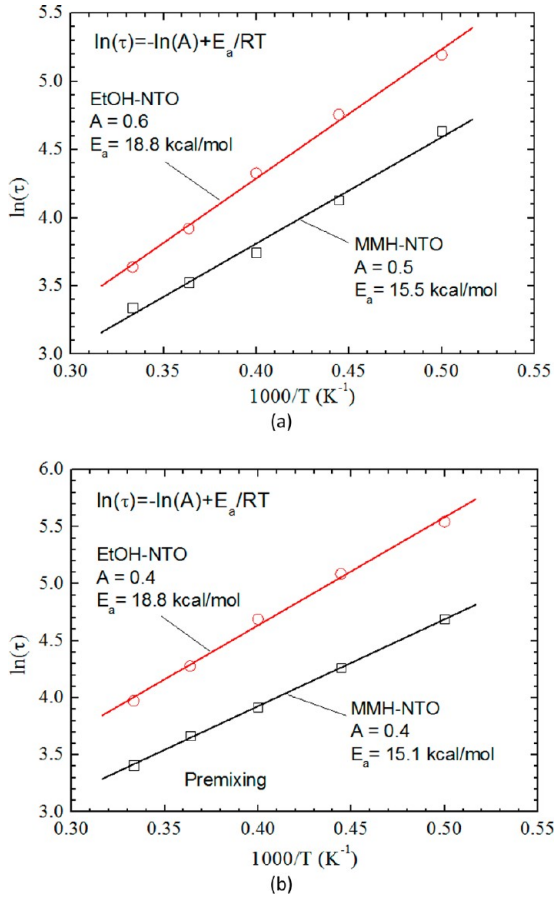

Figure 8. Logarithm characteristic reaction time as a function of inverse temperature (2000−3000 K) for (a) the MMH−NTO and EtOH−NTO without premixing and (b) the MMH−NTO and EtOH−NTO with premixing. The calculated energy barriers of chemical reactions are 15.5 kcal/mol for the MMH−NTO and 18.8 kcal/mol for the EtOH−NTO without premixing, and 15.1 kcal/mol for the MMH−NTO and 18.8 kcal/mol for the EtOH−NTO with premixing, respectively. Insets are Arrhenius equations with fitted parameters.

small slab widths (~30 Å), molecular diffusion is fast enough to establish a good mixing state during chemical reactions, making the reaction barriers calculated in this work close to each other regardless of premixing.

3.6. Statistical Analysis on Chemical Reactions. Chemical reactions occurring in condensed phases often involve a large number of reaction events and types. Thus, it is necessary to analyze the chemical reactions from a statistical point of view to obtain a complete picture of reaction events and channels. We analyzed how many reactions occurring and what types of these reactions are during a period of time. Table 1 and Figure 9 show the number of reaction events, N_r, and the number of reaction types, N_t, that are found in the first 30 ps in NVT dynamics at T = 1000−2000 K. We also calculated the reduced reaction events and types that occur more than four times to ignore rare events. We found that both the number of reaction events N_r and the number of reaction types N_t in the MMH−NTO mixtures are greater than those in the EtOH−NTO mixtures. At T = 2000 K, the reduced reaction events are 70.59% of total reaction events and make up 11.65% of total reaction types in the MMH−NTO mixtures. However, for the EtOH−NTO mixtures, the reduced reaction types are 83.68%

Table 1. Number of Reaction Events (N_{re}) and Reaction Types (N_t) Found in the First 30 ps of the NVT Dynamics at T = 1000−2000 K[a]

	T (K)	full N_r	full N_t	reduced N_r (N > 4)	reduced N_t (N > 4)
MMH−NTO	1000	316	172	86(27.22%)	9(5.23%)
	1250	827	247	546(66.02%)	35(14.17%)
	1500	1466	333	1069(72.92%)	48(14.41%)
	1750	2002	460	1453(72.58%)	63(13.70%)
	2000	3033	747	2141 (70.59%)	87 (11.65%)
EtOH−NTO	1000	201	74	94(46.77%)	7(9.46%)
	1250	572	125	401(70.10%)	17(13.60%)
	1500	1059	177	830(78.38%)	30(16.95%)
	1750	1565	222	1300 (83.07%)	49(22.07%)
	2000	2267	332	1897(83.68%)	66(19.88%)

[a]The reduced reaction events and types are those that occurred more than four times. The values in parentheses are the percentages of reduced N_r with respect to full N_r.

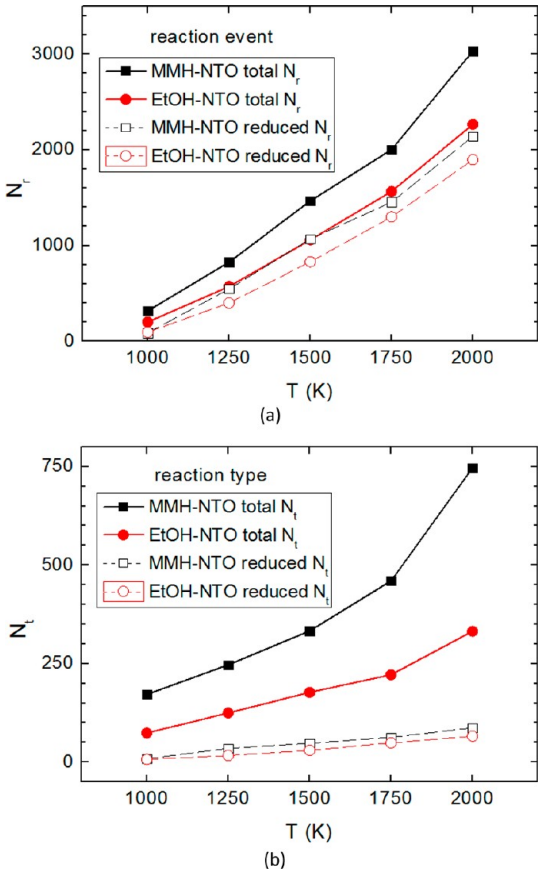

Figure 9. (a) Number of reaction events (N_r) and (b) reaction types (N_t) as functions of temperature analyzed in the first 30 ps of the NVT dynamics at T = 1000−2000 K.

of total reaction events and make up 19.88% of total reaction types. The statistical analyses of reaction events and types indicate that there are more reaction channels in MMH−NTO than in EtOH−NTO.

3.7. Time Evolution of Chemical Reactions. Not only can the numbers and types of reactions be analyzed from reactive dynamics, we can extract information on when a particular reaction type occurs. Figure 10 shows the time

dx.doi.org/10.1021/jp308351g | J. Phys. Chem. B 2012, 116, 14136−14145

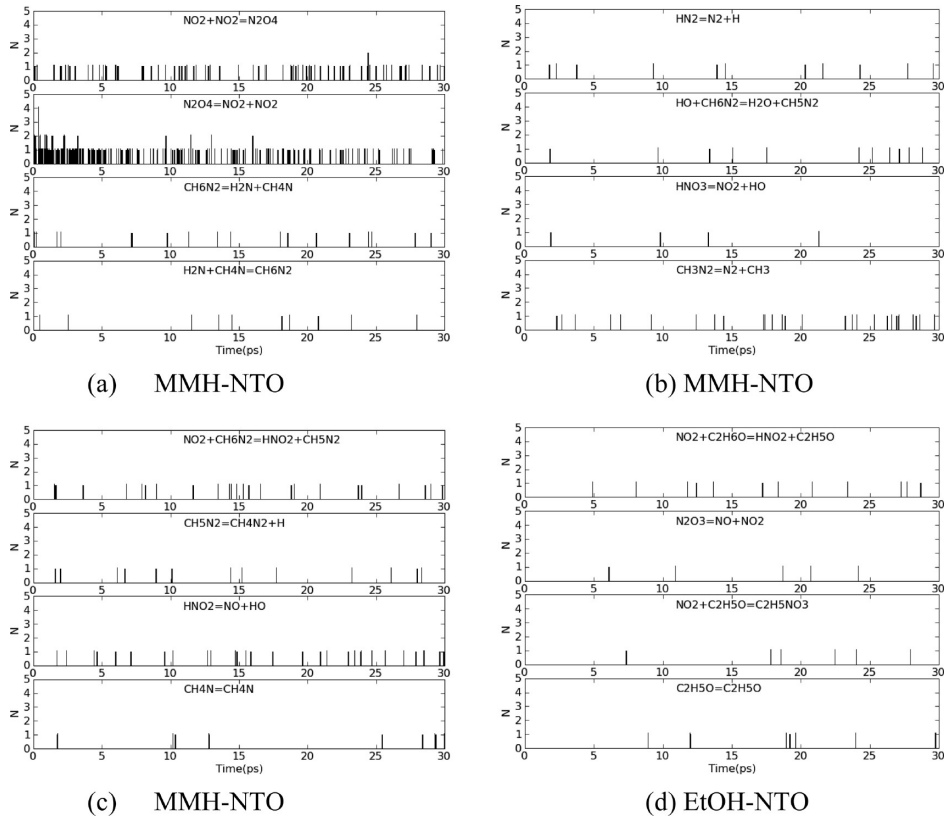

Figure 10. Number of selected chemical reactions as a function of time in the NVE dynamics for (a–c) the MMH–NTO mixture and (d) the EtOH–NTO mixture with an initial T = 2000 K at half densities.

evolution of number of chemical reactions in NVE dynamics with an initial T = 2000 K at half experimental densities. We observed many reactions occurring at a very early stage, e.g., within the first 5 ps for the MMH–NTO mixture. However, few reactions were found for the EtOH–NTO mixture in that time frame. This indicates that the chemical reactions occur earlier in MMH–NTO than in EtOH–NTO.

3.8. Key Reaction Mechanisms. We analyzed and counted the important reaction events within the first 30 ps of NVE dynamics starting from an initial T = 2000 K at half experimental densities. The main early chemical reactions observed in the MMH–NTO mixture are the following. NTO decomposition:

$$N_2O_4 = NO_2 + NO_2(249)$$

Hydrogen abstraction:

$$NO_2 + CH_6N_2 = HNO_2 + CH_5N_2(25)$$

$$NO_2 + CH_5N_2 = HNO_2 + CH_4N_2(12)$$

$$CH_5N_2 = CH_4N_2 + H(13)$$

$$HNO_2 = NO + HO(32)$$

$$HO + CH_6N_2 = H_2O + CH_5N_2(11)$$

N–N bond scission:

$$CH_6N_2 = H_2N + CH_4N(18)$$

$$H_2N + CH_4N = CH_6N_2(10)$$

$$NO_2 + CH_4N = HNO2 + CH_3N(6)$$

The key early reactions observed in the EtOH–NTO mixture are the following. NTO decomposition:

$$N_2O_4 = NO_2 + NO_2(229)$$

Hydrogen abstraction:

$$NO_2 + C_2H_6O = HNO_2 + C_2H_5O(12)$$

$$NO_2 + C_2H_5O = C_2H_5NO_3(6)$$

$$C_2H_5O = C_2H_4O + H(10)$$

$$HNO_2 = NO + HO(8)$$

The counts of each reaction type in the dynamics are shown in the parentheses. We found that more H atoms were abstracted by NO_2 in MMH–NTO than in EtOH–NTO. Furthermore, as shown in Figure 11, among the 25 H abstraction reactions found in the MMH–NTO mixtures, 18 H abstractions occurred for the middle NH, 6 for NH_2, and one for CH_3. However, among the 12 H abstraction reactions of EtOH–OH, 10 H abstractions occurred for OH, one for CH_2, and one for CH_3.

The preferences of H abstraction positions observed in the reactive dynamics agree with our QM calculations. To evaluate the ease of H abstraction, the Mayer bond orders (BO) between N/C/O and H atoms were calculated for MMH and NTO molecules optimized at the DFT/B3LYP level. The BO of the NH, NH_2, and CH_3 of the MMH molecule are 0.905, 0.914, and 0.967, respectively. The small BO indicates weak covalent bonds where H can be easily removed. Indeed, the middle NH in MMH has the smallest BO and was found to lose H most frequently in the dynamics. The BO of the OH,

dx.doi.org/10.1021/jp308351g | J. Phys. Chem. B 2012, 116, 14136–14145

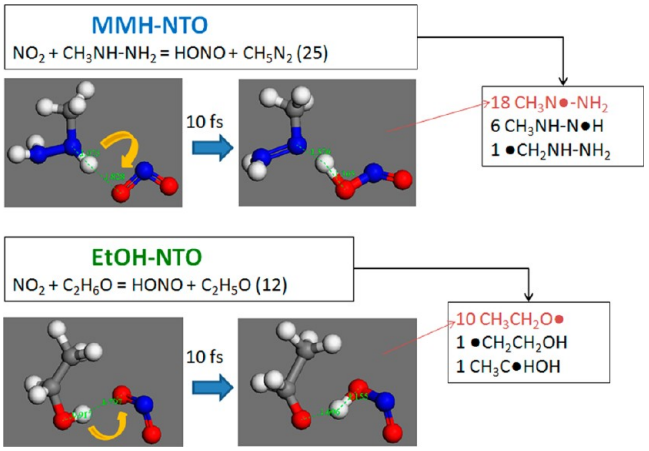

Figure 11. Hydrogen abstraction reactions in the MMH−NTO and the EtOH−NTO mixtures. The numbers are counts of each reaction type found in the first 30 ps of the NVE dynamics with an initial T = 2000 K at half densities.

CH_2, and CH_3 of the EtOH molecule are 0.938, 0.984, and 0.995, respectively. Again, the weakest OH bond tends to lose H in the dynamics more often than the others. As a comparison, the BO of the NN bond in NTO is only 0.538, indicating that the NN bond is weak and that NTO is easily dissociated into two NO_2 molecules. However, the average BO of NO is 1.858; thus, the NO bond in NTO is very strong and is able to extract H from MMH or EtOH molecules.

Besides NO_2, OH radicals can also abstract the H of MMH molecules, which was not observed for the EtOH molecule. Moreover, we found that MMH can have N−N bond scission reactions, but no C−C or C−O bond scissions were found for EtOH. Overall, the MMH−NTO mixture has more reaction channels and reaction events than EtOH−NTO, consistent with the hypergolic behavior of the MMH−NTO mixture.

3.9. Spatial and Temperature Distributions of Products. Figure 12 shows the distribution of chemical species across the interfaces of the mixtures in the first 30 ps of the NVE dynamics with an initial T = 2000 K at half experimental densities. It shows that most NTO decompose into NO_2 in the first 30 ps in both mixtures. The number of NO_2 molecules maximizes at 20 ps due to the interplay between NTO decomposition and NO_2 consumption in reactions with the fuels. We found that NO_2 oxidizer molecules diffuse into the MMH or EtOH side before reacting with these fuels. This suggests that physical transport plays an important role in the kinetics of chemical reactions. The inefficient mixing of two liquids could be a rate-limiting step during the whole reaction kinetics. For the MMH−NTO mixture, 69% of the original MMH molecules decomposed after 30 ps, while only 19% EtOH decomposed in the EtOH−NTO mixture.

Figure 13 shows the probability and spatial distributions of temperatures of NO_2 molecules in NVE dynamics with an initial T = 2000 K at half experimental densities. We found that the majority of NO_2 molecules are below 2000 K and are located at the NTO side, while a few NO_2 molecules are beyond 4000 K and found at the interface of the MMH−NTO mixture. While most NO_2 molecules are relatively cold, a few NO_2 become very hot before reacting with MMH molecules at the interfaces. However, such hot NO_2 molecules are rarely found at the interfaces of EtOH−NTO mixtures. The temperature rises localized at the interface of mixtures are correlated with the interfacial chemical reactions.

4. CONCLUSIONS

In this work, we reported the first ReaxFF dynamics study for the mixtures of fuel MMH/EtOH and oxidizer NTO, demonstrating that the rich information extracted from reactive

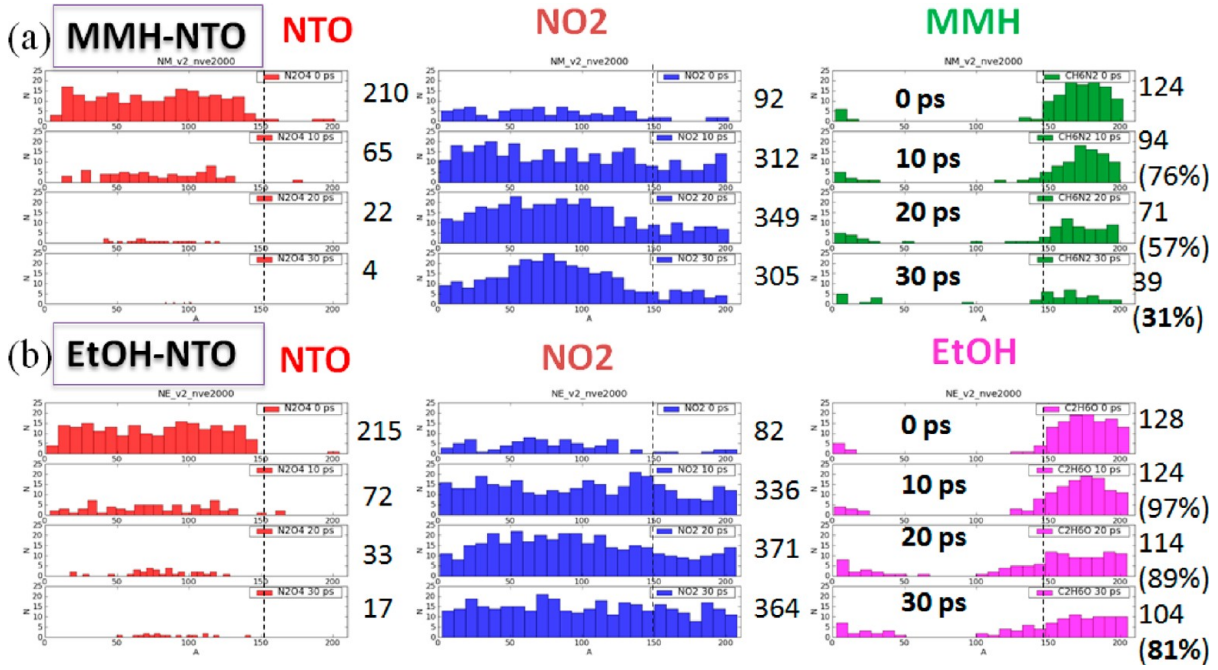

Figure 12. Spatial distributions of the number of chemical species across the interfaces of (a) the MMH−NTO and (b) the EtOH−NTO mixtures (left, NTO; middle, NO_2; right, MMH or EtOH). The numbers are counts of each species found in the NVE dynamics with an initial T = 2000 K at half densities. The vertical dashed lines indicate the initial interfaces between MMH/EtOH and NTO.

dx.doi.org/10.1021/jp308351g | J. Phys. Chem. B 2012, 116, 14136−14145

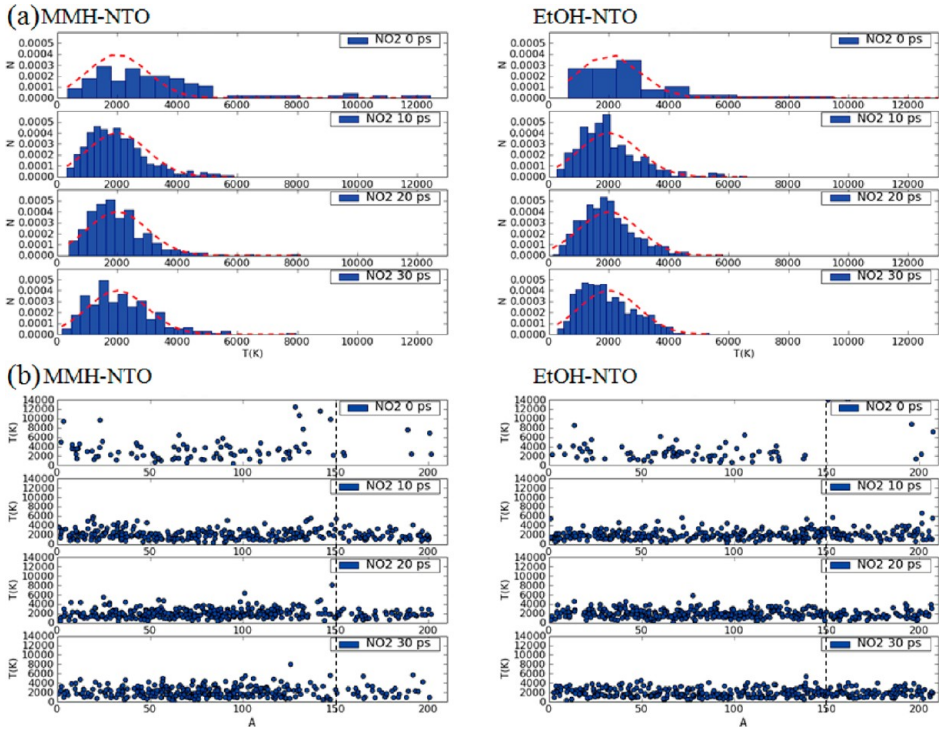

Figure 13. (a) Probability histogram of the temperatures of NO_2 molecules and (b) the spatial distributions of NO_2 temperatures across the interfaces of the MMH−NTO and the EtOH−NTO mixtures. The results are taken from the first 30 ps of the NVE dynamics with an initial T = 2000 K at half densities. The vertical dashed lines indicate the initial interfaces between MMH/EtOH and NTO.

dynamics can provide valuable insight into the microscopic physical processes and chemical mechanisms of hypergolic propellants. We found that the hypergolic MMH−NTO mixture releases more energy at a higher reaction rate and has a lower energy barrier compared to the nonhypergolic EtOH−NTO mixture. In addition, the MMH−NTO mixture is found to have more reaction channels and events than the EtOH−NTO mixture. The hydrogen abstractions and N−N bond scissions are critical early chemical reactions upon mixing MMH and NTO. The search for novel effective propellants should target the molecules with lower energy barriers of H abstractions and bond scissions. Also, selecting small oxidizer molecules with large diffusion mobility can prompt efficient physical mixing to facilitate chemical reactions and increase the chance of the chemical system being hypergolic.

AUTHOR INFORMATION

Corresponding Author

*E-mail: YiLiu@usst.edu.cn (Y.L.); wag@wag.caltech.edu (W.A.G.).

Notes

The authors declare no competing financial interest.

ACKNOWLEDGMENTS

This research received support from ARO (W911NF-05-1-0345; W911NF-08-1-0124), ONR (N00014-05-1-0778), and Los Alamos National Laboratory (LANL). Some computations in this work were carried out on the Army HPC system (the Arctic Region Supercomputer Center). We thank Dr. Betsy Rice and Larry Davis for their assistance. This work was also supported by "Shanghai Pujiang Talent" program (Grant No. 12PJ1406500), Science and Technology Commission of Shanghai Municipality, "Recruit Program of Global Expert" ("Thousands plan") in Shanghai, and the Open Grant of State Key Laboratory of Explosion Science and Technology, Beijing Institute of Technology, P. R. China (Grant No. KFJJ12-6M). Some computations were carried out using the high performance computing facilities at the University of Shanghai for Science and Technology (USST).

REFERENCES

(1) Hurlbert, E.; Applewhite, J.; Nguyen, T.; Reed, B.; Zhang, B. J.; Wang, Y. *J. Propul. Power* **1998**, *14*, 676−687.
(2) Wang, S.; Thynell, S. T.; Chowdhury, A. *Energy Fuels* **2010**, *24*, 5320−5330.
(3) Wang, S. Q.; Thynell, S. T. *Combust. Flame* **2012**, *159*, 438−447.
(4) Catoire, L.; Chambreau, S. D.; Vaghjiani, G. L. *Combust. Flame* **2012**, *159*, 1759−1768.
(5) Catoire, L.; Chaumeix, N.; Paillard, C. *J. Propul. Power* **2004**, *20*, 87−92.
(6) Pichon, S.; Catoire, L.; Chaumeix, N.; Paillard, C. *J. Propul. Power* **2005**, *21*, 1057−1061.
(7) Zhu, J.-F.; He, L.; Zhang, L.; Huang, M.; Tao, G.-H. *J. Phys. Chem. B* **2012**, *116*, 113−119.
(8) McCrary, P. D.; Beasley, P. A.; Cojocaru, O. A.; Schneider, S.; Hawkins, T. W.; Perez, J. P. L.; McMahon, B. W.; Pfeil, M.; Boatz, J. A.; Anderson, S. L.; et al. *Chem. Commun.* **2012**, *48*, 4311−4313.
(9) Zhang, Y.; Gao, H.; Joo, Y.-H.; Shreeve, J. N. M. *Angew. Chem., Int. Ed.* **2011**, *50*, 9554−9562.
(10) Zhang, Y.; Shreeve, J. N. M. *Angew. Chem., Int. Ed.* **2011**, *50*, 935−937.
(11) Schneider, S.; Hawkins, T.; Ahmed, Y.; Rosander, M.; Hudgens, L.; Mills, J. *Angew. Chem., Int. Ed.* **2011**, *123*, 6008−6010.
(12) Schneider, S.; Hawkins, T.; Rosander, M.; Vaghjiani, G.; Chambreau, S.; Drake, G. *Energy Fuels* **2008**, *22*, 2871−2872.
(13) Lecourt, R.; d'Herbigny, F. X. *Aerosol Sci. Technol.* **2004**, *8*, 207−217.
(14) Catoire, L.; Chaumeix, N.; Pichon, S.; Paillard, C. *J. Propul. Power* **2006**, *22*, 120−126.

(15) Osmont, A.; Catoire, L.; Klapoetke, T. M.; Vaghjiani, G. L.; Swihart, M. T. *Propellants, Explos., Pyrotech.* **2008**, *33*, 209−212.
(16) Sun, H.; Law, C. K. *J. Phys. Chem. A* **2007**, *111*, 3748−3760.
(17) Lai, K.-Y.; Zhu, R.; Lin, M. C. *Chem. Phys. Lett.* **2012**, *537*, 33−37.
(18) Liu, W.-G.; Dasgupta, S.; Zybin, S. V.; Goddard, W. A., III. *J. Phys. Chem. A* **2011**, *115*, 5221−5229.
(19) Ishikawa, Y.; McQuaid, M. J. *J. Mol. Struct.* **2007**, *818*, 119−124.
(20) Nonnenberg, C.; Frank, I.; Klapotke, T. M. *Angew. Chem., Int. Ed.* **2004**, *43*, 4586−4589.
(21) Frank, I.; Hammerl, A.; Klapotke, T. M.; Nonnenberg, C.; Zewen, H. *Propellants, Explos., Pyrotech.* **2005**, *30*, 44−52.
(22) van Duin, A. C. T.; Dasgupta, S.; Lorant, F.; Goddard, W. A. *J. Phys. Chem. A* **2001**, *105*, 9396−9409.
(23) Strachan, A.; van Duin, A. C. T.; Chakraborty, D.; Dasgupta, S.; Goddard, W. A. *Phys. Rev. Lett.* **2003**, *91*, 098301−098304.
(24) Strachan, A.; Kober, E. M.; van Duin, A. C. T.; Oxgaard, J.; Goddard, W. A. *J. Chem. Phys.* **2005**, *122*, 054502−054511.
(25) Luzheng, Z.; Zybin, S. V.; van Duin, A. C. T.; Dasgupta, S.; Goddard, W. A. *AIP Conf. Proc.* **2006**, *845*, 589−592.
(26) Zhang, L.; Zybin, S. V.; van Duin, A. C. T.; Dasgupta, S.; Goddard, W. A., III. In *Shock Compression of Condensed Matter*; Furnish, M. D., Elert, M., Russell, T. P., White, C. T., Eds.; American Institute of Physics: New York, 2006; Vol. *845*; p 589.
(27) Zhang, L.; Zybin, S. V.; van Duin, A. C. T.; Dasgupta, S.; Goddard, W. A., III. In *Shock Compression of Condensed Matter*; Furnish, M. D., Elert, M., Russell, T. P., White, C. T., Eds.; American Institute of Physics: New York, 2006; Vol. *845*; pp 585.
(28) Zybin, S. V.; Goddard, W. A., III; Xu, P.; van Duin, A. C. T.; Thompson, A. P. *Appl. Phys. Lett.* **2010**, *96*, 081918−081920.
(29) Budzien, J.; Thompson, A. P.; Zybin, S. V. *J. Phys. Chem. B* **2009**, *113*, 13142−13151.
(30) Han, S.-P.; van Duin, A. C. T.; Goddard, W. A., III; Strachan, A. *J. Phys. Chem. B* **2011**, *115*, 6534−6540.
(31) An, Q.; Zybin, S. V.; Goddard, W. A., III; Jaramillo-Botero, A.; Blanco, M.; Luo, S.-N. *Phys. Rev. B* **2011**, *84*, 220101−220105.
(32) An, Q.; Liu, Y.; Zybin, S. V.; Kim, H.; Goddard, W. A. *J. Phys. Chem. C* **2012**, *116*, 10198−10206.
(33) Zhou, T.-T.; Huang, F.-L. *J. Phys. Chem. B* **2011**, *115*, 278−287.
(34) Zhou, T.; Zybin, S. V.; Liu, Y.; Huang, F.; Goddard, W. A., III *J. Appl. Phys.* **2012**, *111*, 124904−124914.
(35) Wu, C. J.; Fried, L. E.; Yang, L. H.; Goldman, N.; Bastea, S. *Nat. Chem.* **2009**, *1*, 57−62.